Transcutaneous Ultrasound Loading of Piezoelectric-Driven Hernia Repair Mesh For Soft Tissue Healing

By
© 2021

Victoria A. Drapal
B.S., University of Nebraska-Lincoln, 2017

Submitted to the graduate degree program in Bioengineering and the Graduate Faculty of the University of Kansas in partial fulfillment of the requirements for the degree of Master of Science in Bioengineering.

_____
Chairperson Elizabeth Friis, Ph.D.

_____
Candan Tamerler, Ph.D.

_____
Jennifer Robinson, Ph.D.

Date Defended: 21 December 2021

The thesis committee for Victoria Drapal certifies that this is the approved version of the following thesis:

Transcutaneous Ultrasound Loading of Piezoelectric-Driven Hernia Repair Mesh For Soft Tissue Healing

_____

Chairperson Elizabeth Friis, Ph.D.

Date Approved: 26 January 2022

Abstract

Annually in the United States, over one million hernia repairs surgeries occur. A hernia is a painful medical impediment where a portion of soft tissue protrudes through a damaged section of abdominal wall. The only real treatment for hernias is to repair and strengthen the injured abdominal lining. Hernias have a high recurrence rate which leads to surgeons utilizing surgical mesh to help strength the repair and reduce the recurrence rate. However, the use of synthetic mesh in hernia repairs can lead to recurrence rates due to rips or tears along the tissue and biomaterial interface, which leads to additional patient discomfort and difficulties. The recurrence rate for the first-time open hernia repair is 24% even with the use of a hernia repair mesh.[1] Any patient can develop a hernia in their lifetime no matter age, physical condition, or demographic however, certain risk factors can increase a patient's chances of a hernia occurrence such as obesity, tobacco use, and heavy lifting.

Electrical stimulation (ES) for soft tissue repair and regeneration has shown promise in low voltage applications. However, for internal soft tissue regeneration, battery packs would be cumbersome and may require additional surgeries for removal. Low voltage can be made possible through piezoelectric discs that have the unique property of producing current through mechanical loading and thus does not need a battery pack. Therefore, a method of using ES as a conduit for soft tissue regeneration has been proposed. This novel biomedical product concept and the resulting viability will be explored in this thesis work.

The piezoelectric-driven hernia repair mesh was assessed through biocompatibility and viability outcomes. Here, the hernia repair mesh was turned into an electrode through applying a thin layer of gold by sputter coating. The voltage source was a piezoelectric element that was activated through transcutaneous ultrasound loading to provide better healing prospects. The

results from this study show viability of NIH 3T3 cells *in vitro* after 5-, 7-, and 14-days of stimulation. Overall viability results showed promise for the product concept after 5- and 7-days of stimulation. An unexpected complication in the electrode arose in the 14-day stimulation group. Limitations of the work and future work is discussed.

Acknowledgements

My thesis work would not have been possible without guidance, love, and continuous encouragement from friends, family, mentors, and lab-mates. I would like to thank each individual and group for the reinforcement given throughout my time at KU working on my thesis.

Funding Sources

I would like to thank the many different funding sources that allowed me to pursue my education at KU. Without financial support it would not have been possible for me to achieve these milestones. Thank you to the Bioengineering Program, Electrical Engineering Department, Chemical & Petroleum Department, and Mechanical Engineering Department for the many opportunities to share in my knowledge of engineering coursework through Graduate Teaching Assistantships. I would also like to thank the KU Go Grant, Graduate Research Funding, Sustainable Heartland Accelerator Regional Partnership Hub, and Tuition Assistance Program Funding for the ability to continue my research with financial support.

Spine Biomechanics & Structural Biomaterials (SB^2) Lab

Next, I would like to thank everyone in the SB^2 lab for ongoing support and laughs: Craig Cunningham, Ember Krech, Morghan Alters, Ryan Downing, Josh Koski, Zach Pessia, Colton Lowe, Jordan Gamble, Anna Norman, Luke Lindemann, Chris Tacca, Morgan Riley, and Savannah Mosier. Whether it was brainstorming, ranting, or laughing, you all were there to lend a hand, and I will be forever grateful.

Family & Friends

My family & friends were the ones that encouraged me to pursue graduate education, and in turn, convinced me to strive for my graduate degrees. Thank you for seeing success in me when I could not see it myself. I will always be grateful for the strong foundation you gave me in creating

the world around me. Thank you for letting me explain my work and discover ways to better communicate my findings.

Dillon Drapal

Countless thank-you's to my husband, Dillon Drapal. Through thick and thin, you have always been my number one supporter. When a bachelor's degree seemed too difficult, you convinced me that I could do it and now I've accomplished so much more. You have helped me grow as a person, engineer, and scientist. You truly believe that I can do anything I set my mind to which allows me to accomplish more than I thought possible. When Imposter Syndrome kicks in, you are there to quiet those doubts. Thank you for the constant coffee refills, strength during quarantine, and always being my number one fan.

Dr. Candan Tamerler & Dr. Jenny Robinson

Thank you to my thesis committee for allowing me to defend my thesis work here at KU. It has been an honor working with you and bettering myself as an engineer. Dr. Tamerler and Dr. Robinson, thank you for all the guidance throughout the duration of my master's degree. Whether in the classroom or during meetings, you have helped me become a better researcher and shaped the way I see the world.

Dr. Lisa Friis

Lisa, thank you for believing in my capabilities to pursue this work. I found it exciting from the very beginning and I look forward to seeing where the future of this work goes. Thank you for sharing your passion for helping patients with me and allowing me to dive deeper answering these scientific questions.

This page is intentionally left blank.

Table of Contents

Abstract iii
Acknowledgements v
List of Figures ix
List of Tables x
List of Abbreviations xi
List of Equations xii
Chapter 1. Introduction 1
Chapter 2. Soft Tissue Healing: Hernia Repair Background and Literature Review 3
2.1 At-Risk Populations 4
2.2 Hernia Tear Symptoms 5
2.3 Hernia Repair Surgery 5
2.4 Hernia Repair Mesh 6
2.4.1 Synthetic Hernia Repair Mesh 9
2.4.2 Biological Hernia Repair Mesh 10
2.4.3 Composite Hernia Repair Mesh 11
2.5 Soft Tissue Regeneration 11
2.5.1 Electrical Stimulation 12
2.6 Piezoelectricity 13
2.6.1 Piezoelectric Elements for Soft Tissue Applications 14
2.7 Ultrasound Properties 15
2.7.1 Diagnostic Ultrasound 16
2.7.2 Therapeutic Ultrasound 16
Chapter 3. Proof-of-Concept Electrically Active Hernia Repair Mesh Study Design 18
3.1 Material and Methods 19
3.2 Results 27
3.3 Discussion 29
3.4 Conclusion 31
3.5 Study Design Limitations 32
Chapter 4. Conclusion and Future Work 34
Thesis References 38
Appendix 41

List of Figures

POC Hernia Repair Mesh Study Design

Figure 1: Experimental Study Design Setup (a) Overall study design (b) Ultrasound transducer, phantom, and piezo disc setup. 19

Figure 2: (a) Tissue phantom made from Humimic® Gelatin #0 and Metamucil® (b) Single piezo disc encapsulated to a petri dish with silicone. *Scale bars are 2 cm.* 20

Figure 3: Current density calculations of the smaller dimension mesh (20 x 60 mm) with n = 3 (blue) and the larger dimension mesh (24 x 80 mm) with n = 6 (red). 22

Figure 4: Fluorescent images of all experimental groups. *Scale bar 1.5 mm.* 27

Figure 5. Brightfield images of all experimental groups. *Scale bar 100 µm.* 28

Figure 6. The polystyrene 6-well plate after 14-day stimulation study. Gold particles were found in Live/Dead images and are visible to the naked eye in the wells. 30

Figure 7. Microscope images of the gold sputter coated mesh with the gold fully attached to the PP mesh (left image). Gold missing on the mesh (right image). 30

Appendix Images

Figure 8. (a) Initial design for electrode, (b) Mesh glued with 3M VetBond™, (c) Mesh glued with 3M VetBond™ with NIH 3T3 cells and media, (d) 3M VetBond™ patterns used in (c). 46

Figure 9. 3M VetBond™ application made it difficult to distinguish between cells and glue. Large glue clumps can be seen on (a) mesh and 6-well plate, (b) 6-well plate with a distinct line, and (c) combined mesh and 6-well plate. 47

Figure 10. Falcon tube cut to a height of 18 cm to push the mesh to the bottom of the 6-well plate. 47

Figure 11. Initial tests with 3M VetBond™ showed bubbles forming and getting caught in the pores of the mesh. 48

Figure 12. DAPI stain to determine if cells were adhering to the mesh. 48

List of Tables

POC Hernia Repair Mesh Study Design

Table 1. Wetting ladder percentages of ethanol to Mill-Q water. 24

Table 2. Temporal viability study experimental groups. 25

Table 3. The number of repetitions per experimental group and the size of the respective mesh. 29

List of Abbreviations

AC	Alternating Current
AFM	Atomic Force Microscopy
Au	Gold
$BaTiO_3$	Barium Titanate
BMI	Body Mass Index
CLACS	Compliant Layer Adaptive Composite Stacks
DC	Direct Current
DMEM	Dulbecco's Modified Eagle's Medium
ECM	Extracellular Matrix
ES	Electrical Stimulation
FBS	Fetal Bovine Serum
FGF	Fibroblast Growth Factor
GSC	Gold Sputter Coated
HIFI	High Intensity Focused Ultrasound
HRM	Hernia Repair Mesh
IAP	Intraabdominal Pressure
KU	University of Kansas
LIDC	Low-Intensity Direct Current
PenStrep	Penicillin Streptomycin
POC	Proof-of-Concept
PP	Polypropylene
PS	Polystyrene
PZT	Lead Zirconate-Titanate
qPCR	Quantitative Polymerase Chain Reaction
SEM	Scanning Electron Microscopy
TE	Tissue Engineering
TM	Topography Microscopy
VPC	High-Voltage Pulsed Current
WSES	World Society of Emergency Surgery

List of Equations

Hernia Repair Mesh Equations

Laplace's Law

$$tension = \frac{(diameter\ x\ pressure)}{(4\ x\ wall\ thickness)} \quad (1)$$

Current Density Equations

$$V_{rms} = \frac{V_p}{\sqrt{2}} \quad (2)$$

$$P = \frac{V_{rms}^2}{R} \quad (3)$$

Ohm's Law

$$I = \frac{V}{R} \quad (4)$$

$$\rho = \frac{j}{v} \quad (5)$$

Chapter 1. Introduction

A painful medical impediment is the development of a hernia where part of an organ, such as part of an intestine, protrudes through weakened abdominal wall and thus needs repair to prevent further damage. Any patient can develop a hernia in their lifetime no matter age, physical condition, or demographic. Certain risk factors can increase a patient's chances of a hernia occurrence which includes obesity, tobacco use, and heavy lifting.

Current treatments start with monitoring symptoms to determine severity of hernia. However, the only treatment of a hernia once it has developed is hernia repair surgery. Since the 1980's most hernia surgeries involve the use of a hernia repair mesh (HRM) to help strengthen and support the compromised tissue and promote healing. However, while multiple HRM have been engineered, there still lacks a truly optimal mesh style for the best repair of all hernia types.

Electrical stimulation (ES) has shown promise in faster healing prospects at low level voltage for some soft tissue healing applications like skin regeneration. Depending on location of the hernia, soft tissue regenerative practices is hypothesized to have the same beneficial effects. This approach is novel and worth investigating due to the unique properties of ES such as infection protection and promotion of natural healing.[25] Other investigation into infection resistance has shown that antimicrobial coating is not very effective. Therefore, a novel product concept of combining the soft tissue healing benefits of low-level electrical stimulation with a gold sputter coated (GSC) polypropylene (PP) HRM will be explored.

The aim of this thesis work was to determine the efficacy through cellular viability of a GSC piezo-integrated HRM for soft tissue regeneration via ultrasonic transcutaneous mechanical loading for healing purposes after surgery. The metrics for determining the viability of the device was Live/Dead Assay (Thermo Fisher, Waltham, MA) *in vitro* on the medical grade PP surgical mesh (PPKM505 0.125 mm monofilament, 1.3 x 1.5 mm pores 58 GSM, SurgicalMesh™ Division, Textile Development Associates, Inc.). The study design includes viability at one ultrasound

intensity (0.5 W/cm^2) of the temporal effects after 5-, 7-, and 14-days of stimulation. The temporal viability experimental groups were 1) PP mesh, no ES, (2) GSC PP mesh, no ES, and (3) GSC PP mesh, ultrasound intensity 0.5 W/cm^2. Each experimental group underwent 5-, 7- and 14-days of stimulation, twice daily. The number of repetitions in each experimental group was a total of three for this POC viability ultrasound intensity test (n = 3).

The results of this study showed promise for low-level ES for the application of hernia repair surgery after 5- and 7- days of stimulation. The viability of the 5-day GSC HRM also indicated more cells adhered to the mesh compared to the two control groups (PP mesh and GSC mesh, no ES) after the same time duration. The GSC HRM showed problems with flaking and nonadherence to the PP mesh.

Overall, this work demonstrates the need for a HRM that provides better healing prospects then current commercially available selections provide. While there are three main types of commercially available products, synthetic, biological, and composite, each one trades positive attributes to compensate for losses. The ultrasonic transcutaneous mechanically loaded HRM would provide faster healing prospects for a patient population that is currently suffering.

Chapter 2. Soft Tissue Healing: Hernia Repair Background and Literature Review

Hernias occur when a part of an organ, such as the intestines, protrudes through a compromised section of the abdominal wall and thus needs repair to prevent further damage.[2, 3] Hernias happen due to trauma or underlying issues that leads to the weakening of the abdominal wall.[3] In the United States alone, hernia repair surgeries exceed one million annually.[4, 5] The estimated global hernia repair procedures are around 20 million surgeries annually.1[2] Hernias are hindersome and can cause patients additional complications such as chronic pain, adhesion, and infection.[3] There are two main classifications of hernias categorized by the World Society of Emergency Surgery (WSES) that refer to the location of the hernia anatomically: (1) groin hernias and (2) ventral hernias.[3] Furthermore classification of groin surgeries involves hernias that occur in the lower half of the torso such as indirect inguinal, direct inguinal, and femoral hernias.[6] Ventral hernias further incorporates the wide range of other types of hernias such as umbilical, epigastric, Spigelian, lumbar, and incisional hernias. [3, 6] The most common type of hernia, occurring 70-75% of hernia cases, is the inguinal hernias.[2]

While patient monitoring is the first step in hernia diagnosis, the only treatment for a hernia is surgery to repair and close up the damaged tissue.[6] There are three types of hernia repair that typically occur: laparoscopic repair, laparoscopic transitioned to open, and open surgery.[5] From the 1890s through the 1980s sutured repairs dominated as the traditional fixation device.[6] Unfortunately, complications often arose with too much tension on the suture line that led to recurrence of the hernia.[6] Now each of these types of repairs can and often include the use of surgical repair mesh, depending on the location of the tear and patient condition.[2] The frequency of HRM has increased since the 1980s, for example, over 90% of groin hernia repair surgeries now use mesh.[5] The recurrence rates of an incisional hernias have decreased from 17-67% to 1-

32% when surgical repair mesh has been used.[7] However, other hernia surgeries reports have the recurrence of a hernia due to the synthetic HRM which leads to additional patient discomfort and difficulties. Recurrence rates in the most common type of hernia repair, ventral hernia repair, range from approximately 24% to 43%.[1, 8]

In addition to the patient pain and discomfort physically, there is also the monetary cost burden. The estimated cost for groin and ventral hernias combined is $10 billion annually.[3, 9] Costs associated with these recurrences are approximately $700 million annually for United States hospitals.[8, 10] Hospitals bear the burden of the time in the operating room, recovery room, and facility associated with a herniorrhaphy.[11]

2.1 At-Risk Populations

The at-risk patients for hernia occurrences encompass a wide range of the population. Factors associated with the development of hernias can be related to physical wellbeing, genetic traits, or acute trauma. These factors can be heavy weightlifting, abnormal strain while excreting, pregnancy, obesity, genetic conditions, and any activity that requires excessive pressure inside the abdomen.[3, 6] Activities such as long-term, chronic constipation and strain to have a bowel movement, chronic coughing or sneezing, cystic fibrosis, tobacco use, and overexertion can lead to a higher chance of developing a hernia during lifetime.[6]

Unfortunately, there can be hernia cases where the cause of the torn tissue is not clear. Hernias can even be present at birth but not present until later in life.[6] The various types of hernias can also have increased risk due to gender. Examples of hernias that are a higher risk of developing for males s inguinal hernias. Whereas for females, there is a higher risk of developing a femoral hernia.[6] The bottom line is that anyone can develop a hernia in their lifetime.

2.2 Hernia Tear Symptoms

Symptoms of hernia tears can be discomfort or pain but typically patients report that there are no symptoms.[6] However, patients that do have symptoms may complain of a bump that is growing and sore.[6] In specific situations, when a hernia gets too large, it can outgrow the hole of the intestine and therefore be cut off from its blood supply. These cases are called strangulation; strangulation causes pain and swelling for the patient.[2] Other symptoms of hernia strangulation are nausea, vomiting, and not being able to pass gas or have bowel movements.[6]

2.3 Hernia Repair Surgery

The first step of hernia repair is to evaluate the level of hernia size and determine the level of patient pain. However, the only true treatment for a hernia is surgery.[6] A surgeon will enter the abdominal cavity and repair the weakened tissue (fascia) and close the hole that was created by the bulging tissue. Specific technique utilized by clinician and hernia repair fixation device is determined by the practicing clinician, although typically occurs with the Lichtenstein technique (often called the “tension-free” technique) and with sutures or HRM.[2, 6]

There are a few methodologies developed overtime that can be utilized by clinicians to repair the hernia. The first is the choice between open or laparoscopic surgery. Open surgery allows for the clinician to open the abdominal wall the access the hernia location and repair the problematic area with HRM. Open surgeries can lead to infection at the hernia location site. Laparoscopic surgery, where a small incision is made, decreases the risk of infection for the patient but has mixed results as far as pain management.[3]

The most common surgical procedure to repair a hernia is through the Lichtenstein surgical method. This procedure is when the surgeon closes the obstruction with one of the

various fixation devices through making a hole just above the hernia.[3] This method aids in the disruption of the tension caused by the placement of mesh inside the abdomen.[12, 13] An additional parameter while using the Lichtenstein surgical procedure is to set the mesh 2 - 4 cm beyond the boundary of the inguinal triangle also called the Hesselbach's triangle.[14]

The location of the HRM is determined by the clinician and specific to each patient condition. The anatomy of the abdominal cavity includes skin, subcutaneous tissue, muscle tissue, and peritoneum. The various mesh fixation locations vary depending on the abdominal plane. The main three locations of fixation are onlay, inlay, or sublay positions.[3] Onlay implantation occurs when the mesh is placed between the subcutaneous tissue and the anterior rectus sheath, sublay is when the mesh is placed below the rectus muscle (between the posterior rectus sheath and rectus muscle or between the peritoneum and posterior rectus sheath or muscle) and, lastly, inlay implantation is when the mesh is placed between the edges of the layer of abdominal tissue specific to where the hernia defect is located.[3] Location fixation is determined by the clinician with ample guideline provided by the Americas Hernia Society (AHS), European Hernia Society[15], or the WSES.[16]

2.4 Hernia Repair Mesh

HRM has had many different iterations throughout the years and continues to be developed to better enhance certain beneficial qualities. Stemming from metal sutures, one of the original design concepts for HRM mesh was to use a silver filigree, developed by Phelp, Goepel, and Witzel in 1900 to increase the integrity of the damaged tissue.[17] The unfortunate and major design flaw was the silver particles formed poisonous silver sulfate within the abdominal cavity. It additionally had weak mechanical properties of being stiff and fragile. Metals of similar mechanical characteries were then developed (Stainless Steel and Tantalum) and utilized since the

poisonous silver sulfate was not formed, but the negative mechanical properties still plagued the design. In 1959, the first synthetic mesh was proposed by Kootnz that had infection resistance properties. Other materials such as Nylon, Polyvinyl sponge silicon, Orlon cloth, and Teflon were also discovered and utilized.

Due to the sheer quantity of HRM products, there are many different variations on how to classify them so that clinicians can better identify the specific mesh for each unique hernia. Efforts include categorizing them based off the main material skeleton, mechanical properties, and/or biological properties. The most broad and current method categorizes HRM into three types that exist on the market: synthetic, biological, and composite mesh.[3] Each have unique advantages and disadvantages which makes the selection process all the more difficult since parameters such as type of mesh, patient condition, and properties have to be considered. While there are gains and losses of each type of mesh, each one is still used clinically and is determined by clinician selection. Recent meshes have also included drug coating applications to help with bacterial infections such as loading antibacterial agents such as Rifampicin onto the surface of the converted hydrophilic PP mesh which showed promising results.[18]

The rate of recurrence after the inclusion of mesh and proper fixation decreased to below 5%, but not without additional complications arising.[3] HRM introduced the increased chance of mesh migration, chronic pain, infection, and seroma formation.[3] The mesh itself is held in place either with surgical tacks, sutures, tissue glues, or staples that are found in other types of surgeries to secure the mesh until optimal tissue integration is acquired.[3] Full integration is considered achieved on average 2-3 week post-surgery.[3] The timeframe where the mesh is considered to be the most fragile is called the Howe's Latency Period.[17] This time period is from one to two weeks postoperative. With all the advancements there is still no clear conduit as to

perform the repair surgeries in an open or laparoscopic fashion, what selection of mesh to utilize, or which anatomic plane the mesh should be placed for the optimal hernia repair surgery.[9]

For a hernia mesh to be successful, the mechanical strength must not exceed nor be inferior to the physiological strength of the abdominal wall. This phenomenon can be calculated using Laplace's law (**Equation 1**).[2, 3] This law states that within an elastic spherical vessel (such as the abdomen) the variables of tension, diameter, pressure, and wall thickness must be taken into account.[3]

$$tension = \frac{(diameter\ x\ pressure)}{(4\ x\ wall\ thickness)} \quad (1)$$

For example, the maximum amount of pressure that is seen within the walls of the abdomen by either coughing or laughing on average is 170 mmHg.[3, 19, 20] Whereas the minimum amount of pressure seen was 2 mmHg.[19] There was also a high correlation between higher body mass index (BMI) and increased intraabdominal pressure (IAP).[19] Depending on the performed activity the IAP changes constantly; a patient laying down (supine position) has an average IAP of 2 mmHg, then sitting increases the IAP to 16.7 mmHg, and finally standing increased the pressure to 20 mmHg. One of the most commonly employed synthetic meshes is polypropylene (PP)[21]; heavy weight PP can withstand ten times the maximum amount of abdominal pressure, but the properties change once inserted into the body due to the surrounding host tissue.[3] The change in properties of the mesh cause additional engineering design complications. A worsening of hernia repair mesh tensile strength overtime can lead to future hernia recurrences and worse functional results.[2] Due to the variation in properties, there is an abundance of options to choose from. In 2018, there was a reported 70-80 various types of synthetic HRM commercially available for clinicians.[17] This makes the task of selecting the optimal mesh, specific to patient condition, a particularly daunting and challenging obstacle.[17]

2.4.1 Synthetic Hernia Repair Mesh

There are numerous synthetic mesh options on the market which cover a broad range of biomaterials. According to Brown and Finch, there are three main properties that determine which biomaterial to use: type of filament, tensile strength, and porosity.[22] For example, porosity determination developed by Earle and Mark aims to create a mesh standardization.[21] Here the categories are very large pore (>2000 μm), large pore (1000-2000 μm), medium pore (600-1000 μm), small pore (100–600 μm) and micro porous pore (<100 μm).[21] Sanders *et al* includes five additional criteria in determining the optimal mesh: biocompatibility, risk of infection, handling convenience, socioeconomic, and longevity.[23] Where biocompatibility incorporates a wide range of key properties such as being physically and chemically inert, harmless, reinforces and resists mechanical strain, permits normal physiological function, is nonallergic, is nonmigratory, does not adhere to the viscera, is a noncarcinogen, and is capable of causing or predicting biological response.[17] The weight of the mesh is another criteria that has been placed into subcategories, such as heavy-weight (>80 g/m^2), medium-weight (50-80 g/m^2), light-weight (35-50 g/m^2) and ultra-light-weight (<35 g/m^2).[2] Brown and Finch claim that in most hernia repair situations, a surgeon should select a mesh that is light-weight, large pores, and minimal surface area.[22]

Many biomaterials have been engineered to attempt to meet these criteria, but depending on the material, some positive properties are enhanced but other times sometimes new complications can arise. Some polymeric meshes composed of polymers that have been used either by themselves or in mixtures are polyglactin, polyglycolic, polypropylene, polyester, ePTFE, collagen, cellulose, PVDF, sodium, polyglecaprone, titanium, omega-3, tantalum, stainless steel, marlex, prolene, dacron, polytetraflouroethylene, dexon, vicryl, and vypro.[21, 22]

Whichever properties encompass the various synthetic mesh chosen, there are categories that they can be further classified: macroporous, microporous, and macroporous meshes with multifilament or microporous components.[3] Additional properties include the pattern of filaments such as knitted or woven which indicate porosity, density, and flexibility.[3]

These biomaterials vary in advantages specifically flexibility, great mechanical properties, and biocompatibility. Additionally, synthetic mesh is inexpensive to produce making it a promising mesh for application. However, there are a lot of disadvantages to using synthetic mesh, specifically, increased risk of inflammation, stiffness, high infection rate, and fistulae.[3] These shortcomings lead to further patient pain and discomfort.

2.4.2 Biological Hernia Repair Mesh

Biological meshes are unique due to the nature of fabrication. Production of these meshes comes from the decellularized extracellular matrix (ECM)-based scaffolds of allogenic (autograft or allografts) or xenogenic origin.[2, 3] Animal intestine submucosa or pericardium have also been utilized.[2, 3] Once decellularized, the scaffold contains the remnants of the dermis complex collagen matrix and then can be used for hernia repair.[2, 3] The native cells of the patient can infiltrate the already organized collagen matrix and use the scaffold for the repair by generating connective tissue that can replace the damaged tissue of the hernia.[2] Of utmost importance is that the body incorporates the mesh (both synthetic and natural polymers) eventually as its own so that no major infection resistance is evoked by the host. Natural polymers in literature have shown to not have such a negative host response, especially if the natural polymer is an autograft or allograft (compared to a xenograft), but reaction can still occur.[2]

The advantage to this mesh is low inflammation rates, low formation of fistulae, and a reduced fibrosis.[3] This can be attributed to the concept that host cells infiltration of the collagen

matrix for recolonization and revascularization.[2, 3] However, biological mesh produce lower mechanical strength while also being extremely expensive to produce.[3] Studies are still determining if compromise of lower mechanical strength is worth the high price.

2.4.3 Composite Hernia Repair Mesh

Aiming to combat the issues that arise with synthetic and biological HRM, composite mesh was created to address key design flaws common in both types of mesh. Composite HRM, often with a PP backbone paired with another synthetic material or natural polymer, has a dualism design where the properties of the top and bottom of the mesh differ.[2, 3] One side of the mesh (visceral side) is smooth and microporous that aims to prevent adhesion.[2, 3] The other side of the mesh (abdominal side) is rough and microporous to encourage infiltration of tissue.[2, 3] This mesh design concept requires a certain implantation arrangement due to the engineering design. An example of composite HRM is the TiMeshTC® (Gfe Medizin-technik, Nuremberg, Germany) where patients with the titanium mesh had quicker rates of returning to work and quicker rates of normal activity.[24]

The advantages to composite HRM are low fistulae formation.[3] The addition of coatings can aid in the non-adhesion properties, but inflammation can still occur.[3] Which leads to the main disadvantage of composite HRM, the introduction of various degrees of inflammation.[3]

2.5 Soft Tissue Regeneration

The human body is a complex system that uses biochemical signals, electrical signals, and mechanical loading to promote healing. Many invasive and non-invasive remedies and treatments for wound healing include compression bandaging, wound dressings, negative pressure wound therapy, ultrasound, debridement, and skin substitutes.[25] However, these

procedures can be time-consuming and yield slow positive results.[25] Literature has advocated for the use of ES together with these standard treatments to hone the healing abilities of ES with the older methods that have been helpful in the past.[25] The literature shows that ES can reduce infection, improve cellular immunity, increase perfusion, and accelerate cutaneous wound healing.[25]

2.5.1 Electrical Stimulation

Similar to bone regeneration through ES, it has been shown that cutaneous wound healing with ES is achievable and beneficial.[25] There are several different ES applications including direct current (DC), alternating current (AC), high-voltage pulsed current (VPC), low-intensity direct current (LIDC), and electro-biofeedback ES.[25] Research into the various types of ES can leave to an inability to generate sufficient evidence to support any one type of ES due to the variation in parameters and type of ES utilized.[25] While it may be difficult to compare and contrast across the varying studies, overall evidence shows that ES leads to significant improvement in the wound area or accelerated wound healing.[25]

The stages of wound healing are haemostasias, inflammation, proliferation, wound contraction, and remodeling.[25] Restoration of skin continuity and function is one of the main metrics for normal wound healing.[25] Undamaged human skin naturally creates an endogenous electrical potential and has a transcutaneous current potential of 10-60 mV.[25] When the wound does not fully heal, a chronic wound develops. Chronic wounds are when the wound has failed to go through the reparative phases of healing in less than 42 days.[25] Factors that can lead to delayed wound healing can be diabetes[26], tobacco use[26], vascular insufficiency, age, and nutritional deficiencies.[25]

An *in vitro* study explored the effects of fibroblasts exposed to ES for a duration of 6 hours.[27] The experimental group that was exposed to ES had a greater number of viable cells than those not exposed to ES.[27] The ES fibroblasts also had an increased speed of migration when a wound was introduced in the culture.[27] The overall conclusion was that the exposure to ES promoted fibroblast growth and wound healing in addition to showing the viability of the cells after ES.[27]

2.6 Piezoelectricity

Piezoelectric elements are best described as a material that exerts a small voltage when a mechanical load is applied to the material. Crystals that do not have a center of symmetry, anisotropic crystals, are classic crystals that exert piezoelectricity.[28] Anatomical structures in the body have naturally exhibited piezoelectric properties specifically, bones contain these properties due to collagen fibers. Therefore, more broadly, a piezoelectric material is an object that produces current when mechanically compressed. Examples of electroceramics are lead zirconate-titanate (PZT) ($PbZr_xTi_{-x}O_3$), which has shown to be the best transducer material and is most widely used piezoelectric ceramic, or barium titanate ($BaTiO_3$), which has shown to be the best high-permittivity capacitor.[29]

Piezoelectric material and elements have been used in a multitude of applications such as gramophones, hydrophones, and other listening devices.[29] Additionally, piezoelectric components have entered the medical field appearing in pacemakers[30], biosensors[30], and immunosensors[28]. Recently, piezoelectric components have also recently been incorporated uniquely into orthopedic applications such as spinal fusion interbody devices.[31-34]

There are various ways of arranging the piezoelectric elements to produce different conductivity patterns in diphasic solids.[35] Ceramic-plastic composites have even been

biomimetically fabricated with a 3-3 phase conductivity after coral.[29] The biomaterial selected to encapsulate the piezoelectric element drives the mechanical properties such as the piezoelectric coefficient (*d* or *g*), density, and flexibility.[35] Ceramic piezoelectric elements are too brittle and stiff to be used for most biomedical applications, whereas a polymer with the correct mechanical properties supplies too weak piezoelectric properties for application; a combination of a polymer and a ceramic allow for mixed properties.[35]

2.6.1 Piezoelectric Elements for Soft Tissue Applications

Piezoelectric elements have been incorporated into biomedical devices throughout the years; examples of such devices are pacemakers and biosensors.[30] More recently, an interbody spinal fusion device that utilizes the unique properties of piezoelectricity exhibited faster bone healing after spinal fusion surgeries.[31, 32] The original concept spinal fusion interbody implant was designed by Tobaben *et al* where macro fibers operating in d_{33} mode were stacked in three layers to promote healing once under mechanical strain.[33] Initial results from this work showed the power output at three distinct stages of device manufacturing.[33] The effects of the number of layers, mechanical preload, load frequency, and amplitude on maximum power, and optimal electrical load resistance were characterized in 2016.[34] After numerous attempts at fiber constructs, an easier-to-manufacture concept of layered piezoelectric stacks and later the addition of compliant layers was developed.[31, 32] Compliant Layer Adaptive Composite Stacks (CLACS) were designed and exhibited better output from the device.[31]

This work demonstrates that piezoelectric materials, like in the case of the spinal fusion interbody device, have the capability of producing low level electrical signals from mechanical loading. Incorporating these concepts together to create an electrically active hernia repair mesh

for faster healing capabilities could be realized. This would eliminate the need for an external battery pack due to the unique mechanical properties that ultrasound waves produce.

2.7 Ultrasound Properties

Ultrasound machines have two main medical applications: diagnostic and therapeutic. More specifically, this can include investigation into abdominal, cardiac, maternal, gynecological, urological, and soft tissue locations.[36] Furthermore, there are four modes of medical ultrasound imaging: A-mode, B-mode, M-mode, and Doppler mode.[36] The first mode, A-mode, uses a single transducer to scan an echo line through the patient's body to create a two-dimensional image.[36] B-mode provides the possibility for a two-dimensional image by scanning a linear array of transducers through the patient's body.[36] M-mode allows for motion to be captured through a swift sequence of B-mode images.[36] The last mode is Doppler mode, where the Doppler effect measures and visualizes fluid flow.[36]

The main components of an ultrasound machine are the transducer, transmitter pulse generator, amplifiers, control unit, digital processors, and display systems; all of these constituents create the whole ultrasound machine unit.[36] Ultrasound waves propagate outwards from the transducer or probe by compressing air and collecting the echo reflected towards the face of the probe.[37] The type of ultrasound transducer components can differ and are often separated into three categories which are piezoelectric, magnetosctrictive, and liquid-driven.[38] The ultrasound transducer that incorporates ceramic piezoelectric crystals act as the active property for ultrasound propagation, sometimes referred to as ferroelectric components.[37, 38] Sound waves are created when an electric field is applied to the piezo crystals and additionally, the opposite occurs when the transducer registers sound waves, it will produce an electric field.

The sounds waves are reflected towards the face of the transducer once encountering boundaries, such as skin, muscle, and fat. In the case of the diagnostic ultrasound machines, these reflections of sound beams can then be converted into electrical signals that are registered by additional components of the ultrasound machine to create an image. Equations that utilize the speed of sound to calculate the distance between the tissues and the probe allow for the traditional two-dimensional image to represent the surrounding area. A three-dimensional image is made possible by compiling multiple adjacent two-dimensional images together.[36] One key parameter in ultrasound usage is the coupling gel placed between the transducer and contact skin. Ample application ensures that no air pockets are introduced as a barrier for the sound waves to transmit, since inaccurate readings and the potential for major signal interference can occur.

2.7.1 Diagnostic Ultrasound

Diagnostic ultrasound is used to determine obstructions located throughout the body in areas where air, such as the lungs, or bones are not capable of interfering with signal. Imaging in a non-invasive method allows for a more informed decision on medical practices. Specifically, diagnostic ultrasound has been used for informed pregnancy monitoring such as growth and development of the fetus. Other diagnostic capabilities include imaging the heart, blood vessels, eyes, thyroid, brain, abdominal organ, or muscles. Tumor detection is made possible through elastography where the stiffness of the target tissue is evaluated. Another use for diagnostic ultrasound is using the imaging as a guide for needle placement within the body.

2.7.2 Therapeutic Ultrasound

The secondary use for ultrasound is for therapeutic means of using the properties of acoustic waves to heat, ablate, or even break up tissues. While the components of diagnostic

ultrasound are still applicable to identify, target, guide treatment, and verify effectiveness of treatment, there are additional perks of operating the acoustic waves of ultrasound. Utilizing high level ultrasounds sound waves to target specific tissues is called High Intensity Focused Ultrasound (HIFI). HIFI provides clinicians a non-invasive way to potentially break up abnormal tissue structures such as tumors. High intensity sound waves also can alleviate pain from bone metastases and treat uterine fibroids.

These ultrasound properties are ideal for mechanically loading the transcutaneous piezo-driven circuit so that no additional battery packs or surgeries are needed. Using a tissue phantom to mimic the attenuation for ultrasound waves within the body, the concept of mechanically loading the implant can be demonstrated by applying therapeutic levels of ultrasound intensity over the course of ten minutes, twice daily.

Chapter 3. Proof-of-Concept Electrically Active Hernia Repair Mesh Study Design

This POC study for hernia repair includes an electrically active HRM that can be stimulated through a tissue phantom with ultrasound waves. The study design demonstrates the NIH 3T3 mouse fibroblast cells viability with one ultrasound intensity (0.5 W/cm^2) after 5-,7-, and 14-days. The NIH 3T3 mouse fibroblast cells were chosen due to literature illustrating the adhesion, proliferation, and migration properties of other biomedical polymers, specifically polyaniline.[39] There are multiple conceptual components that once miniaturized, manufactured, and regulated, could make this novel device unique for faster healing prospects.

Physiological level ES has shown beneficial effects in improving healing in both hard and soft tissue regeneration. Piezoelectric materials have the capability of producing low level electrical signals from mechanical loading to help speed healing.[8] In this presented work, a novel electrically active HRM for faster healing prospects where transcutaneous mechanical loading of the piezo-driven circuit with therapeutic ultrasound is assessed for *in vitro* cellular viability. Therapeutic ultrasound can mechanically load structures in the body via propagation of high frequency (>20kHz) sound waves in tissues. Previous work has shown therapeutic ultrasound can generate sufficient power to mechanically load piezoelectric discs through 20 mm of phantom tissue.[9]

Combining the novelty of piezo elements to create an electrically active HRM for faster healing prospects is conducted in this study through simulated transcutaneous mechanical loading of the piezo element with therapeutic ultrasound. The ultrasound intensity remained constant at 0.5 W/cm^2 and the temporal viability affects at 5-, 7-, and 14-days was conducted. It was hypothesized that an electrically active HRM initiated by ultrasonic mechanical stimulation through a developed tissue phantom[10] could enhance cell viability, adhesion to mesh, and matrix

formation. This presented work evaluates the viability after selected days at one ultrasound intensity.

3.1 Material and Methods

Overall Setup

The overall experimental design setup incorporated the use of an oscilloscope, therapeutic ultrasound, ultrasound probe, tissue phantom, coupling gel, circuit, piezo disc, and polystyrene (PS) 6-well plate (**Figure 1**). The oscilloscope was set to a frequency of 1 MHz and was used to determine the maximum output voltage of the piezo disc. The therapeutic ultrasound was used to mechanically load the piezo through the tissue phantom. The tissue phantom was created to mimic the depth and attenuation of the average United States patient (BMI of 28) undergoing hernia repair surgery. The coupling gel was used to ensure that no air was between the face of the probe and the tissue phantom (**Figure 2a**). Additionally, it was used as a precaution between the tissue phantom and piezo disc. The circuit was designed to incorporate resistances that would be seen in the clinical setting, such as the resistance of skin, tissue, and muscle. A single piezo disc was wired accordingly and encapsulated in a petri dish with silicone (**Figure 2b**). The wire leads from the piezo disc were then attached to the circuit. The final aspect of the study design setup was the PS 6-well plates with the sputter coated HRM electrically in parallel that were then connected to the circuit.

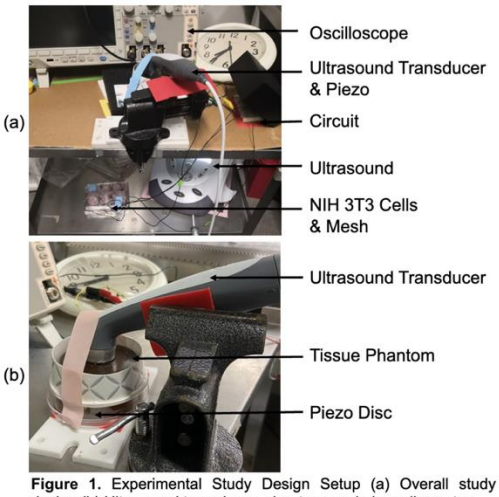

Figure 1. Experimental Study Design Setup (a) Overall study design (b) Ultrasound transducer, phantom, and piezo disc setup.

Circuit Fabrication

The circuit was designed so that multiple resistive components of the human anatomical system would be accounted for and represented on the circuit board. Resistance of the average skin, tissue, and muscle were measured, and the resulting resistance was added to the circuit. Additional caution was also considered for the oscilloscope offset and the appropriate resistance was added.

Tissue Phantom

The tissue phantom mimics the depth of abdominal wall thickness (40 mm) and attenuation that is present in the average United States patient (BMI of 28) undergoing hernia repair surgery. The ability to stimulate the piezo disc through a tissue phantom was previously conducted in the lab.[40] The development of the tissue phantom was demonstrated through 5 experimental groups of various gels and fiber supplements.[41] The tissue phantom that had an attenuation most likely to be seen in the human body is made up of Humimic® medical grade Gelatin #0 and a fiber supplement (Metamucil®) (**Figure 2a**).

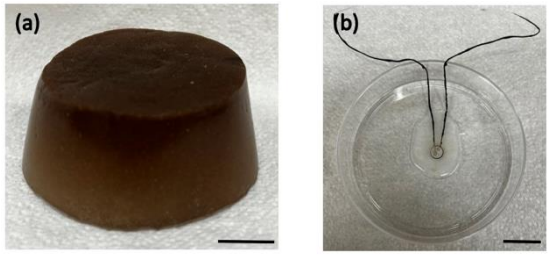

Figure 2. (a) Tissue phantom made from Humimic® Gelatin #0 and Metamucil® (b) Single piezo disc encapsilated to a petri dish with silicone. Scale bars are 2 cm.

Gold Sputter Coating

The polypropylene (PP) mesh (PPKM505 0.125 mm monofilament, 1.3 x 1.5 mm pores 58 GSM, SurgicalMesh™ Division, Textile Development Associates, Inc.) was sputter coated to

create an electrode for ES. The PP mesh was adhered to glass slides using double sided lab tape and placed on the rotating platform of the sputter coater (EMS150R S Quorum). A gold (Au) target was selected to be deposited through sputtering onto the PP hernia mesh based on its conductive capabilities and biocompatibility.[42] The sputter parameters for Au included current (60 mA), chamber pressure ($1x10^{-1}$ Pa), sputter rate (13-20 nm/min), and density (19.32 g/m^3). To ensure the Au was efficiently adhered to the PP mesh when later handled (touched, stretched, or bent), the deposited thickness was set to be 100 ± 10 nm.[43] After the completed deposition, the mesh electrodes were then pressed flat to ensure curvature was prevented.

There were two sizes of PP mesh that underwent sputter coating. The first iteration of sputtering included one specimen with a dimension of 24 x 80 mm. Only one mesh could be gathered from this method. To increase productivity and cost effectiveness, a new method of sputtering was employed where a larger 80 x 80 mm square of PP was sputter coated. Then the subsequent GSC mesh was cut to a smaller and more manageable size (20 x 60 mm), using a rotary cutter to ensure straight and efficient cutting. This method allowed for 5 mesh to be gathered per sputter coater run. The changes in current density due to the size variations and amount of mesh wired in parallel are explored next.

Current Density Calculations

The current density of the HRM changed during the study due to a change in sputter coating methodology. To allow for more mesh per sputter coating session, the size of the mesh decreased. Originally (for the mesh in the 5- and 7-day temporal viability studies) the mesh was 24 x 80 mm in dimension and were ran in sextuplicate ($n = 6$) which allowed for an average current density of 105 nA/cm^2. Only one mesh could fit on the platform per sputter coating session in this arrangement and so the method of sputter coating was reconsidered. The mesh size was

decreased to 20 x 60 mm which resulted in much higher current densities up to 9 times that of the original size (**Figure 3**).

Another change that affected the current density calculations was the decrease from having six samples (n = 6) in a test group and electrically connected in parallel to having only three (n = 3). This decrease in the amount of mesh caused for an increase in the current density since the overall surface area decreased. The decrease in sample size and mesh surface area caused a large increase in current density.

Once the setup was complete, data points from the oscilloscope were collected and ran through a Butterworth filter in a developed MATLAB (MathWorks, Natick, MA) code (**Appendix**) to cancel out the subsequent noise. The current density was calculated with the smaller mesh size and smaller number of repetitions (20 x 60 mm, n = 3) and with the larger mesh size and the larger number of repetitions (24 x 80 mm, n = 6). As expected, the 20 x 60 mm, n = 3 test groups received a higher current density then the 24 x 80 mm, n = 6 test groups (**Figure 3**).

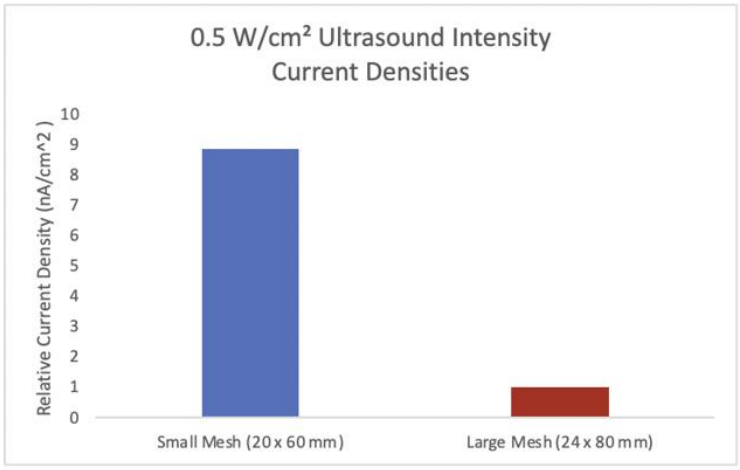

Figure 3. Current density calculations of the smaller dimension mesh (20 x 60 mm) with n = 3 (blue) and the larger dimension mesh (24 x 80 mm) with n = 6 (red).

The equations used to obtain the current density are listed below. The root mean square voltage (V_{rms}) is shown in **Equation 2** where the peak voltage (V_p) divided by the square root of two which results in V_{rms}.

$$V_{rms} = \frac{V_p}{\sqrt{2}} \quad (2)$$

Power (P) (**Equation 3**) is calculated with the square of V_{rms} (**Equation 2**) and divided by the resistance (R).

$$P = \frac{V_{rms}^2}{R} \quad (3)$$

Current (I) (**Equation 4**) is calculated using Ohm's Law where measured voltage (V) is divided by the resistance (R).

$$I = \frac{V}{R} \quad (4)$$

Lastly, to obtain current density (j) (**Equation 5**) through the magnitude equivalent, the root mean square current (I_{rms}) is divided by the cross-sectional area of the mesh. Alternatively, current density can be calculated to determine the vector definition by multiplying the charge density by the velocity of the charges (**Equation 6**).

$$j = \frac{I_{rms}}{A_{cs}} \quad (5)$$

$$j = pv \quad (6)$$

Mesh Sterilization and Wetting Ladder

Once the PP mesh were rotary cut to a dimension of either 24 x 80 mm or 20 x 60 mm they were prepped in surgical bags to be steam autoclaved at 120°C for 30 minutes.[44, 45] The

mesh then underwent a wetting ladder with ethanol and sterilized Mill-Q water to increase hydrophilicity of the hydrophobic PP mesh. The first step of the wetting ladder is to future confirm the mesh sterilization with UV light for 45 minutes. The meshes are laid flat inside a sterile tissue culture hood that was wiped down with 70% ethanol prior to UV radiation. Once the 45 minutes of UV light are concluded, the next processes are the concentrations of ethanol and water. The wetting ladder represents rungs on a ladder where the further along the ladder an increase in water and decrease in ethanol is completed. An incremental increase of water occurs, starting at a concentration of 70/30 of ethanol to sterilized Mill-Q water, until 100% water is achieved (**Table 1**). The mesh was then incubated (37ºC) overnight in 40% fetal bovine serum (FBS) for protein adsorption to promote integrin binding. The prepped mesh was then electrically connected with wires across the mesh and linked to the piezo element that was embedded in silicone.

Table 1. Wetting ladder percentages of ethanol to Mill-Q water.

EtOH/DI H2O Percentages	Overall Volume in Beaker (Cover specimen)	Time in Hood	Ratios EtOH/DI H2O
70/30	100 mL/beaker	30 minutes	70 mL/30 mL
50/50	100 mL/beaker	30 minutes	50 mL/ 50 mL
30/70	100 mL/beaker	30 minutes	30 mL/ 70 mL
0/100	100 mL/beaker	30 minutes	0 mL/ 100 mL

Temporal Viability Studies

The role of the viability study is to determine the temporal effects with NIH 3T3 mouse fibroblast cells (ATTC, Manassas, VA). Additionally, the viability study was to determine the efficacy of the electrically active HRM. For the temporal studies, one ultrasound intensity was chosen (0.5 W/cm^2) and conducted over a period of 5-, 7-, and 14-days (**Table 2**). The metric of viability was a Live/Dead™ Viability/Cytotoxicity Kit (Thermo Fisher Scientific, Waltham, MA)

where two fluorophores indicated the live (calcein-AM) and dead (ethidium homodimer-1) cells. The excitation and emission of calcein-AM is 494/517 nm and for ethidium homodimer-1 in the presence of DNA is 528/617 nm.

Table 2. Temporal viability study experimental groups.

Number	Experimental Group (n=3)	Electrical Loading (Ultrasound Intensity)	Number of Stimulation Days
1	GSC PP Mesh	No ES	5
2	GSC PP Mesh	0.5 W/cm^2	5
3	PP Mesh	No ES	5
4	GSC PP Mesh	No ES	7
5	GSC PP Mesh	0.5 W/cm^2	7
6	PP Mesh	No ES	7
7	GSC PP Mesh	No ES	14
8	GSC PP Mesh	0.5 W/cm^2	14
9	PP Mesh	No ES	14

NIH 3T3 mouse fibroblast cells were plated on PS 6-well plates at 150,000 cells per well for the temporal viability studies, incubated at 37˚C with 50 RPM for 7 hours[46], and then moved to a stationary incubator at 37˚C for the remainder of the study. The media was Dulbecco's Modified Eagle Medium (DMEM) with 10% FBS and 1% Penicillin Streptomycin (PenStrep) where all components were warmed up to human body temperature (37°C) in a water bath so that the NIH 3T3 cells were not shocked by cold media. The media was changed every 3 days, more specifically, the 5-day media was changed once, the 7-day media was changed twice, and the 14-day media was changed fourfold. First, the media was aspirated out of the wells, a warm PBS wash was conducted then aspirated out, and finally the warmed media mixture was placed.

The NIH 3T3 cells on the mesh were loaded electrically via the voltage released by the piezo disc. The piezo disc was mechanically loaded twice daily through a tissue phantom with a clinical/therapeutic ultrasound machine (Chattanooga Intelect TranSport). More specifically, the

ultrasound machine was turned on for 15 seconds and then off for 15 seconds for a total of 10 minutes, twice daily. For the temporal studies, the total length of study was either 5-days (10 stimulation runs), 7-days (14 stimulation runs), or 14-days (28 stimulation runs).

Study Design Setup

Once the mesh has been properly prepped for the NIH 3T3 cells to be plated (sterilized, wetting ladder, 40% FBS overnight soak, wired, and plated with the shaking incubator) the cells were incubated at 37°C and were only taken out to undergo stimulation or to have media changed. The electrically wired HRM is connected to the circuit with the piezo elements and the stimulation can commence. The stimulation takes place twice daily (12 hours apart) where therapeutic ultrasound loads the piezo discs through a tissue phantom developed previously.[41] Over the course of 10 minutes, the ultrasound is turned on for 15 seconds and off for 15 seconds so that the total time of ultrasound loading is 5 minutes.

3.2 Results

The temporal viability studies showed viability with cellular growth on all three experimental mesh groups (PP mesh, GSC mesh, and GSC mesh with ES) (**Figure 4**). The Live/Dead™ Viability/Cytotoxicity assay shows live cells fluorescing green (due to the calcein-AM) and dead cells fluorescing red (due to the ethidium homodimer-1). Over the 5-days of stimulation, the PP and GSC PP controls showed similar amounts of live and dead cells adhered to the mesh. The 5-day GSC PP ES mesh appeared to have more live cells on the mesh then both controls. Over the 7-day study, the PP and GSC PP controls increased in the amount of cellular growth on the mesh compared to the 5-day study. There was a decrease in the amount of dead cells seen on both controls for the 7-day study. The 7-day GSC PP ES group had similar levels of live cells on the mesh and had fewer dead cells compared to the GSC control group.

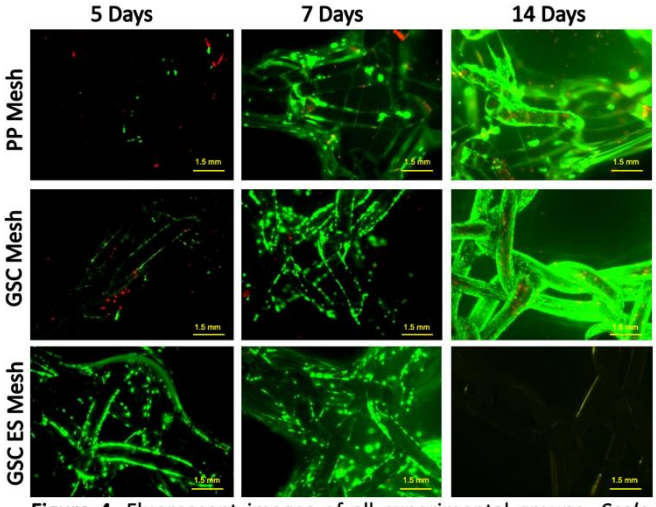

Figure 4. Fluorescent images of all experimental groups. *Scale bar 1.5 mm.*

In the 14-day study, the PP and GSC PP controls had more viable cells compared to the 5- and 7-day control groups, but the GSC PP control group had more cell adherence compared the PP control. The 5-, 7-, and 14-day PP and GSC PP controls showed an increasing amount of

cellular growth on the mesh with a decreasing amount of dead cells fluorescing. The 5- and 7-day ES showed similar amounts of cellular growth on the mesh. However, the 14-day GSC ES did not have any cellular viability. Both controls of the 7-day showed similar amount of viable cells compared the GSC ES mesh. However, there seemed to be more dead cells on the controls then the GSC ES mesh.

There were a lot of black flakes visible in the brightfield images of the GSC with ES groups for 5-, 7-, and 14-day studies (**Figure 5**). The black flakes that appear in the images are gold pieces that have broken off the PP mesh. There was an increase in the amount of black flakes in the 14-day study compared to the 5- and 7-day studies. However, this is not necessarily due to the number of days of stimulation, which will be discussed in the next section.

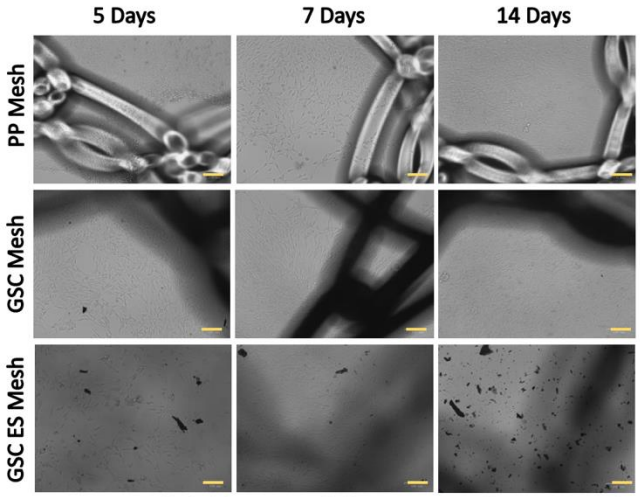

Figure 5. Brightfield images of all experimental groups. *Scale bar 100 µm.*

3.3 Discussion

To accommodate for the large quantity of GSC mesh that needed to be created, halfway through the design process, the size of the mesh was re-evaluated to a smaller dimension. This, in turn, changed the current density value. In addition to the size of the mesh, the number of repetitions was also reduced (20 x 60 mm, n = 3). These two changes allowed for the current density to increase ninefold the original current density seen with the larger mesh with higher repetitions (24 x 80 mm, n = 6). The experimental groups that were not consistent between the studies and can be seen on **Table 3**.

Table 3. The number of repetitions per experimental group and the size of the respective mesh.

Mesh Style	5 Days	7 Days	14 Days
PP Mesh	Smaller Size 20 x 60 mm n = 3	Smaller Size 20 x 60 mm n = 3	Smaller Size 20 x 60 mm n = 3
GSC Mesh	Smaller Size 20 x 60 mm n = 3	Smaller Size 20 x 60 mm n = 3	Smaller Size 20 x 60 mm n = 3
GSC, ES Mesh	Larger Size 24 x 80 mm n = 6	Larger Size 24 x 80 mm n = 6	Smaller Size 20 x 60 mm n = 3

The temporal viability studies showed the NIH 3T3 cells were able to adhere to the GSC PP mesh with ES after 5- and 7-day studies, however the 14-day study did not have cells on the mesh nor in the PS 6-well plates. Referencing **Table 3**, this phenomenon could have occurred due to the change in dimension of the mesh and the number of repetitions. While it should not be overlooked that the possibility the ES was not compatible after 14-days of stimulation, it is not indicative that the ES was the sole cause of the lack of viability.

There was a significant amount of gold flecks in the PS 6-well plate after the 14-day stimulation (**Figure 6**). It is hypothesized that the NIH 3T3 cells adhered to the gold flakes and

were aspirated out during media changes (there were four media changes throughout the course of the 14-day study). In the brightfield images, there are dark flecks that are gold particles from the mesh (**Figure 5**).

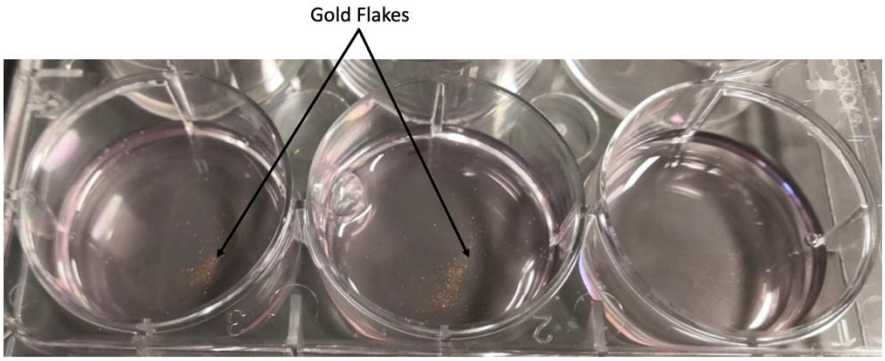

Figure 6. The polystyrene 6-well plate after 14-day stimulation study. Gold particles were found in Live/Dead images and are visible to the naked eye in the wells.

Due to the change in size and change in amount of parallelly connected mesh, the current density changed and could have caused the gold sputter coating to flake off the mesh during stimulation (**Figure 7**). The increase of 10-14 times the current density seen in the 14-day GSC ES studies could have been the reason for the decrease in viable cells. This hypothesis is highly considered since gold flaking is present in additional 2-day studies with the smaller size mesh and the 14-day study of the smaller size mesh (**Table 5**).

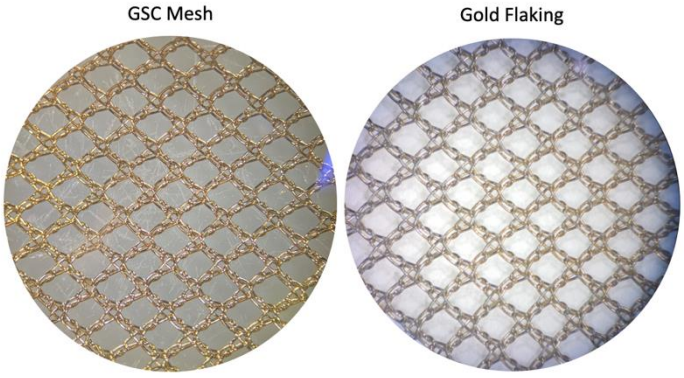

Figure 7. Microscope images of the gold sputter coated mesh with the gold fully attached to the PP mesh (left image). Gold missing on the mesh (right image).

3.4 Conclusion

Overall, the GSC PP mesh had better *in vitro* cellular viability then the plain (non-sputter coated) PP mesh. The temporal viability studies showed that the 0.5 W/cm^2 was a viable intensity for the NIH 3T3 mouse fibroblast cells on the mesh for 5- and 7-days' worth of stimulation. The temporal studies showed that the NIH 3T3 cells were still viable after 14-days on the two controls groups but did not show viability on the 14-day ES group. The phenomenon of no viability on the 14-days' worth of stimulation could have been due to higher current density values, a smaller about of mesh in parallel, or nonviability after that duration of ES. The GSC method of creating the electrode on the HRM was not effective as it flakes off in the process of ES. Future studies could indicate the faster healing prospects provided by the electrically active HRM once the electrode material has a stronger bond to the PP mesh.

3.5 Study Design Limitations

While efforts were made to mitigate design limitations within reason, there was still human error and machine constraints. Some of the study design limitations could be mitigated if the study were to be conducted again. The first would be to conduct the whole experiment with the same number of experimental specimens and limit the number of variations in the study design. There was an uneven number of repetitions ($n = 3$ or $n = 6$) depending on the experimental groups which directly affects the current density. This was to assuage the number of runs of the sputter coater and thus the size of the mesh was also reduced. In turn, this changed the current density provided to the NIH 3T3 cells. When the study is conducted again, the mesh will need to be sputter coated with the correct settings on the sputter coating machine, the size of the mesh needs to remain constant, and the current density and subsequent number of repetitions per experimental group needs to be consistent. The PP mesh will also be washed thoroughly with soap to ensure that no oils from human hands rubs off during the cutting phase. Gloves will be always worn while handing the mesh so that no contaminates interfere with the sputter coating, sterilization, or plating of the mesh.

There are inherent limitations of the ultrasound machine, such that the wave produced by the ultrasound probe is a nonhomogeneous wave. It has a beam nonuniformity ratio of 5:1 which indicates the highest and lowest intensity that would strike the face of the piezo disc. To help combat this limitation, an oscilloscope was used to verify the maximum voltage potential was occurring and the piezo was being stimulate by the ultrasound waves. However, the incorporation of the oscilloscope also leads to a slightly inaccurate reading of the circuitry since it pulls away current into the machine.

And lastly, human error occurred during the study design. While the tissue phantom, boundary, and petri dish were all marked with a line so that they were in the same position each time the setup was assembled, human error is introduced with this method. The transducer was lined up each time so that maximum voltage was reached, but there is variation in that method.

Chapter 4. Conclusion and Future Work

This thesis work was able to determine cytocompatibility of the POC piezoelectric integrated HRM for ES for soft tissue regeneration after 5- and 7-days of stimulation where the mesh size was 24 x 80 mm connected 6 mesh in parallel. While the GSC electrode had design flaws, there was some indication that after 5-days of daily stimulation with an ultrasound intensity of 0.5 W/cm^2 there was more cell growth on the GSC PP ES mesh when compared to the controls of plain PP mesh and GSC PP mesh with no ES. Recommendation for future studies is to determine the cause of the flaking of the GSC on the PP mesh. While the there was some level of effective electrode conductance, over time the Au would flake off with potentially undesirable effects in the patient's body.

While this work showed a POC study on the cellular viability of the ES HRM device compared to two controls (PP mesh and GSC mesh), a better understanding of the PP and gold interface needs to be performed prior to additional research. The deposition of the gold was set to 100 nm for this thesis work which might have been a cause for gold flaking that occurred over the course of the study. A hypothesis proposed is that there was excessive amount of gold deposited onto the surface and the excess layers were promoted off the PP surface during the ES. An additional study where the amount of gold is gradually increased starting at 10 nm up to 120 nm in increments of 10 nm could give an indication on the optimal depth of gold for future applications. The study design could include both a physical scraping of the gold with a hard surface and routine administration of ES to determine strength of bond.

The proposed metrics for this study would include imaging such as cross-sectional imaging, atomic force microscopy (AFM), and scanning electron microscopy (SEM) to determine the stability of the gold on the PP. Each unique type of imaging allows for a better understanding of key elements of stability. Cross-sectional imaging would allow for the gold and PP materials to

be visualized with an angle to determine flaking. SEM imaging provides a two-dimensional view of the surface of the gold sputter coating whereas AFM would give a three-dimensional view of the surface of the GSC mesh. Additional metrics should include electrical connection parameters measurements such as resistance, voltage drop, and calculated current density.

This study should then be conducted again to ensure results that better represent the possibility of this product concept. Better controls should be initiated so that current density is uniform across all experimental groups and repetitions are constant. In addition to the viability work presented, an additional study to illustrate the ultrasound intensity variation viability should be conducted. One of the first signs of wound healing is a collagen matrix for the ECM, a total collagen assay could be performed to demonstrate the healing properties of the electrically active HRM against controls.

Future studies should also explore the rate of healing of the GSC mesh with ES against plain PP mesh and GSC mesh without ES. The rate of healing would indicate the level of effective healing. This could be conducted through a scratch assay to better understand the healing potential of the transcutaneous activation of the PZT. Key wound healing metrics, such as fibroblast growth factor (FGF) amplification through quantitative polymerase chain reaction (qPCR) could be conducted to understand the mRNA.

There are initial metrics for wound healing that give indication for the promise of this device for clinical application. A couple of initial metrics include collagen production (proposed in the repeated cellular viability studies) and qPCR of the key protein FGF (proposed in the scratch assay). Collagen matrix organization is promoted by ES in the proliferative phase of wound healing, where the first phase is inflammation, then proliferation, and finally remodeling phases.[25] Wound healing involves the recruitment of many types of cells, growth factors, and signaling networks. Within this complex system, FGF is recruited to help with the restoration of skin,

specifically FGF-2 is cited to be increased in acute wounds. FGF-2, or basic FGF, has shown to synthesize and deposit various ECM components, have a role in re-epithelialization, and tissue remodeling.[47]

Additional studies with soft embalmed cadavers would allow for a better understanding the anatomical field with the planes of fixation location for better engineered designs. A study design that incorporated the validity of the tissue phantom to better match the physiological condition would allow for more translatable results. In addition, the soft embalmed cadavers would illustrate the product concept logistically.

The invention of a clinically informed biomimetic bioreactor would aid in the ability to discover biocompatibility in a more physiological representative environment. Work towards an alpha prototype for such reactor would be beneficial for soft tissue regeneration applications like this work represents and hard tissue applications as well. The bioreactor would cut down on the amount of time needed for product development in animal models and would provide quicker product concept-to-clinical practice for suffering patients.

Once these studies have been completed, a pilot animal model study should be used to represent the healing capabilities provided by this novel biomedical device. Typically, the purpose of utilizing animal models is to have a demonstration of biocompatibility of the mesh and long-term strength.[48] There are many different types of animal models used for hernia repair studies including pigs, rats, mice, rabbits, and guinea pigs.[48] For future studies, an understanding of desired deliverables expected from an animal study would need to be determined to verify the correct species selection.

While this work has conclusive results for the 5- and 7-day temporal viability studies, more research is needed to better understand the healing properties this novel device could present. The electrode is currently not compatible for a biomedical product and would need to be altered

for this product life to continue. While currently available HRM has some success, an electrically active HRM that uses ultrasonic transcutaneous mechanical loading to power the device could provide faster healing prospects for a patient population that is currently suffering.

Thesis References

1. Misiakos, E.P., et al., *Current Trends in Laparoscopic Ventral Hernia Repair.* JSLS, 2015. **19**(3).
2. Baylon, K., et al., *Past, Present and Future of Surgical Meshes: A Review.* Membranes (Basel), 2017. **7**(3).
3. Wang See, C., T. Kim, and D. Zhu, *Hernia Mesh and Hernia Repair: A Review.* Engineered Regeneration, 2020. **1**: p. 19-33.
4. H, K., *Current options in inguinal hernia repair in adult patients.* Hippokratia, 2011. **15**(3): p. 223-231.
5. Administration, U.S.F.a.D., *Health C for D and R. Hernia Surgical Mesh Implants.* 2018.
6. MedlinePlus, *Hernia*, U.S.N.L.o. Medicine, Editor. 2021.
7. Browne J.A., C.C., Pietrobon R., Bethel M.A., and Richardson W.J., *Diabetes and Early Postoperative Outcomes Following Lumbar Fusion.* SPINE. **32**(20): p. 2214–2219.
8. Poulose, B.K., et al., *Epidemiology and cost of ventral hernia repair: making the case for hernia research.* Hernia, 2012. **16**(2): p. 179-83.
9. Valeriy Shubinets, J.P.F., Michael A. Lanni, Michael G. Tecce, Eric M. Pauli, William W. Hope, Stephen J. Kovach, John P Fischer, *Incisional Hernia in the US: Trends in hospital encounters and corresponding healthcare charges.* The American Surgeon, 2018. **84**(1): p. 118-125.
10. Burger, J.W., et al., *Long-term follow-up of a randomized controlled trial of suture versus mesh repair of incisional hernia.* Ann Surg, 2004. **240**(4): p. 578-83; discussion 583-5.
11. Rutkow, I.M., *Demographic and socioeconomic aspects of hernia repair in the US in 2003.* Surgical Clinics of North America, 2003. **83**: p. 1045-1051.
12. Irving L. Lichtenstein, A.G.S., Parviz K. Amid, *The Tension-Free Hernioplasty.* The American Journal of Surgery, 1989. **157**: p. 188-193.
13. George H Sakorafas, I.H., Christos Nissotakis, Nikolaos Kotsifopoulos, Alexios Stavrou, Constantinos Antonopoulos, George A Kassaras, *Open tension free repair of inguinal hernias; the Lichtenstein technique.* BMC Surgery, 2001. **1**(3).
14. Parviz K. Amid, A.G.S., and Irving L. Lichtenstein, *Open "Tension-free" repair of inguinal hernias: the lichtenstein technique.* Eur J Surg, 1996. **162**: p. 447-453.
15. Alimi, Y., et al., *Mesh and plane selection: a summary of options and outcomes.* Plastic and Aesthetic Research, 2020. **2020**.
16. Society, A.H., *Guidelines*. 2021.
17. Idrees, S., et al., *Surgical meshes – The search continues.* Current Medicine Research and Practice, 2018. **8**(5): p. 177-182.
18. Reinbold, J., et al., *Biodegradable rifampicin-releasing coating of surgical meshes for the prevention of bacterial infections.* Drug Des Devel Ther, 2017. **11**: p. 2753-2762.
19. Cobb, W.S., et al., *Normal intraabdominal pressure in healthy adults.* J Surg Res, 2005. **129**(2): p. 231-5.
20. De Keulenaer, B.L., et al., *What is normal intra-abdominal pressure and how is it affected by positioning, body mass and positive end-expiratory pressure?* Intensive Care Med, 2009. **35**(6): p. 969-76.
21. Earle, D.B. and L.A. Mark, *Prosthetic material in inguinal hernia repair: how do I choose?* Surg Clin North Am, 2008. **88**(1): p. 179-201, x.

22. Brown, C.N. and J.G. Finch, *Which mesh for hernia repair?* Ann R Coll Surg Engl, 2010. **92**(4): p. 272-8.
23. Sanders, D.L. and A.N. Kingsnorth, *Prosthetic mesh materials used in hernia surgery.* Expert Rev Med Devices, 2012. **9**(2): p. 159-79.
24. Koch, A., et al., *Randomized clinical trial of groin hernia repair with titanium-coated lightweight mesh compared with standard polypropylene mesh.* Br J Surg, 2008. **95**(10): p. 1226-31.
25. Ud-Din, S. and A. Bayat, *Electrical Stimulation and Cutaneous Wound Healing: A Review of Clinical Evidence.* Healthcare (Basel), 2014. **2**(4): p. 445-67.
26. McDaniel, J.C. and K.K. Browning, *Smoking, chronic wound healing, and implications for evidence-based practice.* J Wound Ostomy Continence Nurs, 2014. **41**(5): p. 415-23; quiz E1-2.
27. Rouabhia, M., et al., *Electrical stimulation promotes wound healing by enhancing dermal fibroblast activity and promoting myofibroblast transdifferentiation.* PLoS One, 2013. **8**(8): p. e71660.
28. Pohanka, M., *Overview of Piezoelectric Biosensors, Immunosensors and DNA Sensors and Their Applications.* Materials (Basel), 2018. **11**(3).
29. R.E. Newnham, L.J.B., K.A. Klicker, L.E. Cross, *Composite Piezoelectric Transducers.* Materials in Engineering, 1980. **2**: p. 93 - 106.
30. Khare, D., B. Basu, and A.K. Dubey, *Electrical stimulation and piezoelectric biomaterials for bone tissue engineering applications.* Biomaterials, 2020. **258**: p. 120280.
31. Krech, E.D., et al., *Effect of compliant layers within piezoelectric composites on power generation providing electrical stimulation in low frequency applications.* J Mech Behav Biomed Mater, 2018. **88**: p. 340-345.
32. Cadel, E.S., et al., *Stacked PZT Discs Generate Necessary Power for Bone Healing through Electrical Stimulation in a Composite Spinal Fusion Implant.* Bioengineering (Basel), 2018. **5**(4).
33. Tobaben, E.J., et al., *Stacked macro fiber piezoelectric composite generator for a spinal fusion implant.* Smart Materials and Structures, 2015. **24**(1).
34. Goetzinger, N.C., et al., *Composite piezoelectric spinal fusion implant: Effects of stacked generators.* J Biomed Mater Res B Appl Biomater, 2016. **104**(1): p. 158-64.
35. R.E. Newnham, D.P.S., L.E. Cross, *Connectivity and piezoelectric-pyroelectric composites.* Mat. Res. Bull., 1978. **13**: p. 525-536.
36. Carovac, A., F. Smajlovic, and D. Junuzovic, *Application of ultrasound in medicine.* Acta Inform Med, 2011. **19**(3): p. 168-71.
37. Health, N.I.o., *Ultrasound*, N.I.o.B.I.a. Bioengineering, Editor. 2016: United States of America.
38. Alhajhoj, M.E.A.M.a.M.R., *Importance and Applications of Ultrasonic Technology to Improve Food Quality*, in *Food Processing*. 2019. p. 1-16.
39. Rejmontova, P., Capakova, Z., Mikusova, N., Marakova, N., Kasparkova, V., Lehocky, M., Humpolicek, P., *Adhesion, Proliferation and Migration of NIH/3T3 Cells on Modified Polyaniline Surfaces.* Int J Mol Sci, 2016. **17**(9).
40. Alters, M., *Determination of Clinical Efficacy of Ultrasound Stimulation on Piezoelectric Composites for Power Generation Applications*, in *Bioengineering*. 2019, University of Kansas: Lawrence, Kansas.
41. Norman, A., *Determination of a Clinically Relevant Tissue Phantom for Transcutaneous Ultrasound Stimulation of Piezoelectric Discs for Current Density Applications*, in *Bioengineering*. 2021, University of Kansas.

42. Roeder, L.A.G.a.R., *Criteria for the Selection of Materials for Implanted Electrodes.* Annals of Biomedical Engineering, 2003. **31**: p. 879-890.
43. Karankar, P.D.a.V.S., *New Avenues of controlling microbial infections through anti-microbial and anti-biofilm potentials of green mono-and multi-metallic nanoparticles: A review.* Journal of Microbiological Methods, 2019. **167**: p. 1-27.
44. Prevention, C.F.D.C.a., *Steam Sterilization*, C.F.D.C.a. Prevention, Editor. 2016.
45. Udo, I.A., I.A. Onwuezobe, and K.U. Umeh, *Resterilized Polypropylene Mesh for Inguinal Hernia Repair.* Niger J Surg, 2018. **24**(1): p. 19-22.
46. Piggott, M.S.a.D., *Shaking 3T3 Cells: Further Studies on Diffusion Boundary Effects.* Cell, 1974. **3**: p. 207-215.
47. Barrientos, S., Stojadinovic, O., Golinko, M.S., Brem, H., and Tomic-Canic, M. *Growth factor and cytokines in wound healing.* Wound Repair and Regeneration. 2008. **16**: p. 585 - 601.
48. Vogels, R.R.M., et al., *Critical overview of all available animal models for abdominal wall hernia research.* Hernia, 2017. **21**(5): p. 667-675.

Appendix

HRM Temporal Viability Studies Protocol

Initially Seeding Cells:

1. Warm the culture media in the water bath to 37˚C. The culture media needs to contain 10% FBS and 1% Streptomycin.
    a. The FBS and Streptomycin are in the cell culture freezer. Also warm them up in the water bath before mixing them in the media.
2. Calculate how many cells you will need by using the attached Thermo Fisher chart (below).
3. Obtain the 3T3 cells from the liquid nitrogen container. Be careful, LN cold burns on contact with skin. Use the approved gloves to remove the cells. There is a chart to locate where the cells are stored. Pick up the appropriate basket. Let the LN drip over the container for a little bit. Then get the box out. Slowly put the basket back into the LN container.
4. Prepare 9 mL of media in a 15 mL falcon tube. The remaining 1 mL will come from the frozen cells.
5. Once in the tissue culture hood, warm up the cells by taking 500 µL of prepared media over the top. Keep supplying warm media until all of the cells are warmed up and in the 15 mL falcon tube.
6. Centrifuge the 15 mL falcon tube (with counterweight) at 200 RCF for 8 minutes. This creates a pellet of cells on the bottom of the tube.
7. Refresh the media by aspirating the old media out of the falcon tube.
8. Resuspend in fresh warm media (10-12 mL) and place in the T75 flask.

9. Tilt the flask so that the media spreads to the entirety of the T75 flask.
10. Place in the incubator (37˚C) for two days.

	Surface area (cm^2)	Seeding density*	Cells at confluency*	Versene (mL of 0.05% EDTA). Approx. volume	Trypsin (mL of 0.05% trypsin, 0.53 mM EDTA). Approx. volume	Growth medium (mL). Approx. volume
Dishes						
35mm	8.8	0.3×10^6	1.2×10^6	1	1	2
60mm	21.5	0.8×10^6	3.2×10^6	3	3	5
100mm	56.7	2.2×10^6	8.8×10^6	5	5	12
150mm	145	5.0×10^6	20.0×10^6	10	10	30
Culture plates						
6-well	9.6	0.3×10^6	1.2×10^6	1	1	1 to 3
12-well	3.5	0.1×10^6	0.5×10^6	0.4 to 1	0.4 to 1	1 to 2
24-well	1.9	0.05×10^6	0.24×10^6	0.2 to 0.3	0.2 to 0.3	0.5 to 1.0
48-well	1.1	0.03×10^6	0.12×10^6	0.1 to 0.2	0.1 to 0.2	0.2 to 0.4
96-well	0.32	0.01×10^6	0.04×10^6	0.05 to 0.1	0.05 to 0.1	0.1 to 0.2
Flasks						
T-25	25	0.7×10^6	2.8×10^6	3	3	3–5
T-75	75	2.1×10^6	8.4×10^6	5	5	8–15
T-175	175	4.9×10^6	23.3×10^6	17	17	35–53
T-225	225	6.3×10^6	30×10^6	22	22	45–68

Falcon Tube Ring Holders:

1. Small rings of a 50 mL Falcon tube need to be cut to help hold the mesh down to the bottom of the 6-well plate when in solution.
2. Using a bandsaw, make cuts at every 5ml marker to create a ring about 1cm in height.
3. After the required number of rings are cut, use a metal file to smooth out the edges of the cut falcon tube rings.
4. When complete, put the pieces in a surgical bag and label the number of pieces inside.
5. Put the surgical bags, with rings inside, in the autoclave at a temperature of 121ºC for 30 minutes.
6. Once the autoclave is done running, bring the bags back to Dr. Robinson's lab. DO NOT OPEN UNLESS UNDER THE HOOD. These are now considered sterile and therefore should not be opened in non-sterile situations.

Sterilization of Mesh (Autoclave):

1. Put gold sputter coated mesh, dimensions 20mm x 60mm, into a surgical bag.
2. Label the bags with number of mesh located in the surgical bags, the date, and what their intended study.
3. Put the surgical bags, with mesh inside, in the autoclave at a temperature of 121ºC for 30 minutes.
4. Once the autoclave is done running, bring the bags back to Dr. Robinson's lab. DO NOT OPEN UNLESS UNDER THE HOOD. These are now considered sterile and therefore should not be opened in non-sterile situations.

Preparation of Mesh (Wetting Ladder and 40% PBS):

1. UV irradiate for 45 min
    a. Do this in a cell culture hood
2. Wetting ladder (use sterilized water)
    a. Add appropriate volume of the solution with a pipet (**Table 1**)
    b. To remove solution, use an aspirator
    c. Put all the mesh in a container that has a lid (so that when the 40% FBS step comes along, you can put it in the incubator)
    d. Be gentle with the mesh since the gold sputter coating can flake off
3. Remove water and dry for 30 min in hood with hood open to ensure residual ethanol is removed.
4. Add 3 mL 40% FBS media with 1% P/S to the specimens and incubate overnight at 37 C. This allows for protein adsorption before the cells are seeded.

Prepare 6-Well Plates:

1. After the autoclaving and wetting ladder/FBS process, take the mesh and rings to Dr. Robinson's lab.
2. Once fully wet, check the connectivity of each mesh with an LCR monitor.
3. Once under the hood, take the mesh that went through the wetting ladder and sat in 40% FBS overnight and place mesh in each well of the plate.
4. Connect the appropriate wires to each mesh. Make sure that if connecting the mesh to each other, they are connected in parallel.
5. The wells are now ready for cells to be plated. After the cells are plated, place one falcon tube ring in each well over the mesh to keep it against the bottom of the well for the remainder of the experiment.
    a. The plating should be at 300,000 for experiments less than 5 days, and 150,000 for experiments greater than 5 days.

Plating Cells:

1. Take the cells out of the incubator and look at them under the microscope. General rule: Happy cells are spread out, unhappy cells are balled up.
2. If happy cells, calculate how much media + cells you need for your 6, 12, 24, etc well plates. (see Thermo Fischer chart again).
3. The cells will be adhered on the bottom of the T75 flask. Aspirate the media out of the cell.
4. Add PBS to cover the plate to wash the cells (about 10 mL). Let it sit for a couple of minutes to wash it thoroughly.

5. Add Trypsin, just enough to cover the bottom of the T75 flask. This will be about 3 mL. Trypsin is the agent that will remove the cells from the bottom of the flask.
6. Put the flask in the incubator for 10 minutes to allow for the separation to occur.
7. Once the 10 minutes is up, look at the cells under the microscope. They should look rounded/balled up.
8. If yes, continue on to the next step.
9. Add media to the flask to make the total amount up to 10 mL (add 7 mL if you added 3 mL of Trypsin). Media that contains FBS will deactivate the Trypsin.
10. Lightly release the media into the flask and tilt the flask to allow for the media to flow over all the bottom of the flask. Do this a few times to make sure that none of the cells are still adhered to the bottom.
11. Transfer the cells (10 mL) into a falcon tube.
12. Centrifuge the 15 mL falcon tube (with counterweight) at 200 RCF for 8 minutes. This creates a pellet of cells on the bottom of the tube.
13. Aspirate out the old media from the tube. Replenish with fresh media (4 mL).
14. Next use the hemocytometer to count the number of cells in your sample.
    a. Get a micro-centrifuge tube
    b. Add 10 µL of your cells + media to the tube. And 10 µL of Trypan Blue. Mix up and down.
    c. Next, add only 10 µL if mixture to the hemocytometer. It uses capillary action to suck the 10 µL under the cover slip and card.
    d. Bring it over to the microscope and count each 4 by 4 block (highlighted in blue). Take the average of the four blocks to calculate total number of cells.
        i. Use the mechanical tally counter to help with counting the small cells.

ii. Only count the cells that are white, not the ones that are covered in Trypan blue since those cells are dead.

iii. Example calculations: (Resuspended in 4 mL of media)

1. Average of 4 blocks * 10,000 cells (calculation for hemocytometer) * 2 (since half is Trypan Blue) * 4 (since we did 4 mL of suspension)
2. 20 cells * 10,000 cells * 2 * 4 = 1,600,000 or 1.6 million cells total

15. Add the amount of media you need to plate your cells.
16. Next add the cells to the 6, 12, 24, etc well plates. (see Thermo Fisher chart again.)
17. Once plated, place in shaking incubator for 7 hours to help evenly distribute cells across the mesh. Then let sit in the incubated for a few days.

Experimental Protocol:

The cells on the mesh will be loaded electrically via the voltage released by the PZT. The PZT will be loaded with an ultrasound machine for 10 minutes in the morning and 10 minutes in the evening. Typically, 8 AM and 8 PM for the stimulation times. If there are multiple intensities in one experimental run, make sure to turn off the ultrasound machine for 15 minutes between runs and remove the ultrasound probe. When the next run is ready to take place, replace the coupling gel on the ultrasound probe.

1. First, add some coupling gel to the petri dish with the piezo disc, place the phantom over the piezo disc and make sure (by flipping it over) that the gel is spread out over the disc. Line up the phantom with the line on the petri dish.
2. Add the boundary condition, making sure to line up the mark on the boundary condition with the phantom.

3. Turn on ultrasound and oscilloscope.
    a. The outlets are located next to the biological hood on the floor to plug in.
    b. Set the ultrasound to the correct intensity for the study (either 0.5, 1.0, or 2.0 W/cm^2)
4. Use the oscilloscope to line up the ultrasound probe over the piezo. Do this by first adding the coupling gel to the ultrasound probe and then moving the probe around on the phantom until you see the appropriate peaks. Use tape to fasten the probe to the phantom.
5. Spray the second level of the stainless-steel cart with 70% ethanol and wipe down.
6. Retrieve the cells from the incubator and place them on the cart where you just cleaned.
7. Unpack the wires and plug them into the appropriate locations on the circuit board.
8. Watching the clock located on the top of the stainless-steel cart, wait until the second hand reaches 12, and then hit start on the ultrasound machine.
    a. It is also necessary to start a 10-minute timer, typically on your phone, so that you do not over stimulate the cells.
9. Hit the pause button every 15 seconds so that the cells receive 15 second on and 15 seconds off for 10 minutes. The current densities will change with each experimental group.
10. When stimulation is concluded, shut off the ultrasound machine, oscilloscope, pack up the wires to the 6-well plate, put the cells in the incubator, clean off coupling gel on the probe, phantom, and piezo, and wheel the cart over to the storing location.

Initial Renditions of Study Design

The shape of the PP mesh initially was designed to be in the shape of a spoon. This was to allow for the most surface area to be covered by the mesh on the bottom of the 6-well plate. PS 6-well plates have a cylindrical shape and the only part that was needed to be completely covered was the bottom of the well (**Figure 8a**). The handle of the spoon shape was to connect the piezo-driven circuitry to the electrodes.

The mesh is a flimsy material that would not sit at the bottom of the plate, especially with the handle of the spoon sticking out from the well (**Figure 8b**). To accommodate this shape, 3M VetBond™ veterinarian super glue was used to adhere the PP mesh to the bottom of the 6-well plate. There were several patterns of medical grade super glue that were examined (**Figure 8d**). A study was conducted with NIH 3T3 cells to determine the interaction between the cells and the super glue.

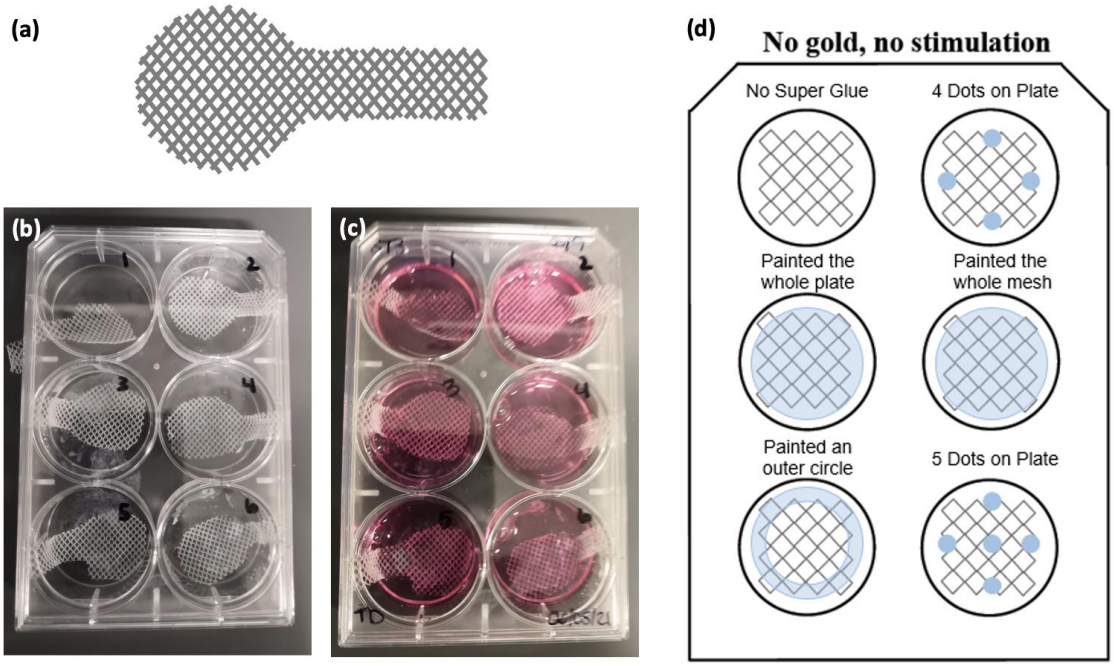

Figure 8. (a) Initial design for electrode, (b) Mesh glued with 3M VetBond™, (c) Mesh glued with 3M VetBond™ with NIH 3T3 cells and media, (d) 3M VetBond™ patterns used in (c).

Ultimately, the super glue made it difficult to see the cells in the well. Even though multiple renditions of application of the medical grade super glue were attempted, the distinction between the NIH 3T3 cells and glue was hard to differentiate (**Figure 9**). The VetBond™ would get stuck on the mesh and clog up the pores. None of the gluing patterns were determined to be effective and ultimately the design switched to falcon tubes to physically hold down the mesh in place instead of fixing the mesh to the bottom of the well.

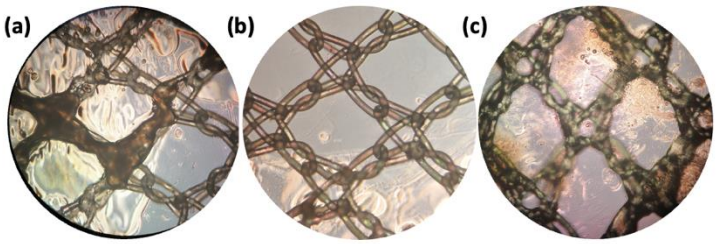

Figure 9. 3M VetBond™ application made it difficult to distinguish between cells and glue. Large glue clumps can be seen on (a) mesh and 6-well plate, (b) 6-well plate with a distinct line, and (c) combined mesh and 6-well plate.

Falcon tubes were cut with a bandsaw so that a height of ~18 cm was achieved. The height of the cut falcon tube was to ensure that the mesh was held to the bottom of the 6-well plate. This was accomplished by making the tube tall enough so that when the lid was placed on top, the mesh was pushed to the bottom of the well (**Figure 10**).

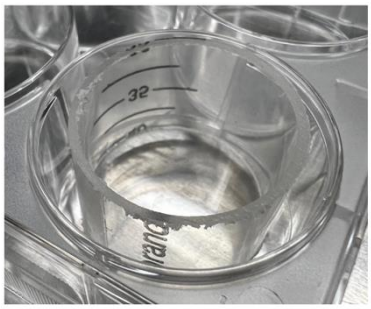

Figure 10. Falcon tube cut to a height of 18 cm to push the mesh to the bottom of the 6-well plate.

Initial tests showed difficulty with obtaining bubbles in the pores of the mesh (**Figure 11**). These air bubbles were formed in the experimental groups with VetBond™ and without VetBond™. Literature showed that shaking the media with cells for 6-8 hours after plating helped get rid of these air bubbles and help the cells spread out more uniformly in the well. The plated cells were then set inside an incubator at 37°C for 7 hours shaking at 50 RPM for the remainder of the studies.

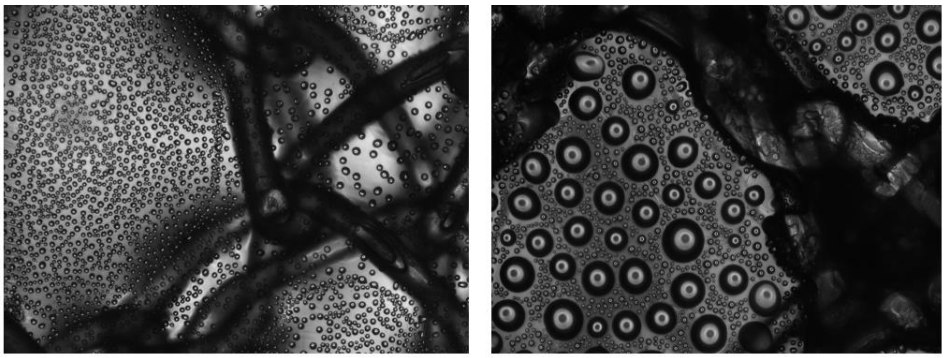

Figure 11. Initial tests with 3M VetBond™ showed bubbles forming and getting caught in the pores of the mesh.

To determine if NIH 3T3 cells were adhering to the mesh, a 4′,6-diamidino-2-phenylindole (DAPI) stain was utilized (**Figure 12**). DAPI is a blue fluorescent that stains DNA in cells. DAPI is effective to both live and dead cells. Early results from the preliminary DAPI stain showed promising results that cells would adhere to the mesh.

Figure 12. DAPI stain to determine if cells were adhering to the mesh.

Oscilloscope Filtering MATLAB Code

```
%% Main Code for Analyzation of Ultrasound Single Disc PZT
% Written by Victoria Drapal
% Adapted from code originally written from Ember Krech
% Last updated: 10/19/2021

%% Notes
% Change each time this code is ran: (1) Change the filename to reflect
% proper Oscilloscope data to read (2) Change the final output name.

%% Clean Command Window & Workspace
clear;close all; clc;

%% File Reading & Naming
filename = ['Day7_6.csv'];    % Change each time code is ran!
Oscilloscope_data_array = table2array(readtable(filename)); % Creating a matrix from the table in Excel

%% Input Parameters (Shouldn't Change Unless Circuit Values Change)
Circuit_Resistance = [1000];                % Resistance is the circuit that can be changed for current density
purposes
Cutoff_Frequency = 1.2e6;                   % Cutoff Frequency

%% Setting iResistor Loop
for iResistor = 1:length(Circuit_Resistance)
Rmuscle=10;                             % Resistance the differential probe measures across to mimic muscle
resistance

%% Setting Variables
Rvar= Circuit_Resistance(iResistor);          % Resistance value in ohms
% Time & Voltage Data from Oscilloscope
time = Oscilloscope_data_array(21:end,1);      % Units are Seconds
voltage = Oscilloscope_data_array(21:end,2);    % Units are Volts
Centered_Voltage = voltage - mean(voltage);     % Center data around zero
raw_voltage(:,iResistor) = Centered_Voltage;    % All raw voltage data
% Sample Frequency Calculation
DeltaT= diff(time);                     % Sample frequency (dertivative of time)
DeltaT_mean = mean(DeltaT);                 % Mean of DeltaT
fs=1/DeltaT_mean;                       % (100Ms/sec): 100 megasamples per second this is set on the
oscilloscope

%% Filtering the Data
[Numerator,Denominator] = butter(5,2*Cutoff_Frequency/fs); % (Nth order, cutoff frequency)how to
determine cutoff freq
Vosc = filtfilt(Numerator,Denominator,Centered_Voltage);
R_total = Rvar + Rmuscle;                   % Total impedance of the ciruit
```

```
Vosc1 = Centered_Voltage.*(1/sqrt(2));        % Convert to RMS voltage
Vout = Vosc1.*((1+(Rvar/Rmuscle)));           % Scale voltage by the applied resistance - find voltage produced
by the specimen
P = Vout.^2./(Rvar + Rmuscle);                % Instantaneous power of circuit
Pavg = trapz(time,P) * 1./(max(time) - min(time));    % Average power
Pavg_uw = Pavg.*(10^6);                       % Pavg converted to microWatts
Vpp = (max(raw_voltage(:,iResistor)) - (min(raw_voltage(:,iResistor))));  % Peak-to-peak voltage (amplitude)
Vamp = Vpp./2;                                % Amplitude of voltage
Vrms = Vamp.*(1/sqrt(2));                     % Vrms measured for the voltage drop across the 10ohm resistor
Pmax = Vrms.^2./(R_total);                    % Peak power per cycle
Pmaxu = Pmax*(10^6);
Pmuscle_max = (Vrms.^2./Rmuscle).*10^6;       % Instantaneous power of muscle resistor

%% Store data to Output
output(iResistor,:)={R_total, Vpp, Pavg, Pavg_uw, Pmaxu, Pmuscle_max, Vrms};

end

%% Plotting the Filtered Data
tiledlayout(1,2)

ax1 = nexttile;
plot(time, voltage)
title(ax1, 'Unfiltred Data')
xlabel('Time(Seconds)')
ylabel('Voltage (Volts)')

ax2 = nexttile;
plot(time, Vosc)
title(ax2, 'Filtred Data')
xlabel('Time(Seconds)')
ylabel('Voltage (Volts)')

%% Output to an Excel for Later Analysis
output_header = {'Resistance (ohm)' 'V P-P (V)' 'Pavg (W)' 'Pavg (uW)' 'Pmax (uW)' 'Pmuscle_max (uW)' 'Vrms
(V)'};
output_final = [output_header; output];
% Writing the output into the Excel file and creating the file
writecell(output_final, ['Filtered_Oscilloscope_Data_Day7_6.xlsx']);   %Change the name each time file is ran!

% Displaying That The Code is Finished Running
fprintf('Little Sneak Peek of %s Data!\n\n',filename)
displayname = table(R_total, Vpp, Pavg, Pavg_uw, Pmaxu, Pmuscle_max, Vrms);
disp(displayname)
disp('Code is done processing! Go to your MATLAB file an
```